Quick Shear-Flow Alignment of Biological Filaments for X-ray Fiber Diffraction Facilitated by Methylcellulose

Takaaki Sugiyama,[†] Daisuke Miyashiro,[†] Daisuke Takao,[†] Hiroyuki Iwamoto,[‡] Yasunobu Sugimoto,[§] Katsuzo Wakabayashi,[§] and Shinji Kamimura[¶*]

[†]Department of Life Sciences, Graduate School of Arts and Sciences, The University of Tokyo, Tokyo, Japan; [‡]Research and Utilization Division, Japan Synchrotron Radiation Research Institute, Hyogo, Japan; [§]Division of Biophysical Engineering, Graduate School of Engineering Science, Osaka University, Osaka, Japan; and [¶]Department of Biological Sciences, Faculty of Science and Engineering, Chuo University, Tokyo, Japan

ABSTRACT X-ray fiber diffraction is one of the most useful methods for examining the structural details of live biological filaments under physiological conditions. To investigate biologically active or labile materials, it is crucial to finish fiber alignment within seconds before diffraction analysis. However, the conventional methods, e.g., magnetic field alignment and low-speed centrifugations, are time-consuming and not very useful for such purposes. Here, we introduce a new alignment method using a rheometer with two parallel disks, which was applied to observe fiber diffractions of axonemes, tobacco mosaic tobamovirus, and microtubules. We found that fibers were aligned within 5 s by giving high shear flow (1000–5000 s^{-1}) to the medium and that methylcellulose contained in the medium (~1%) was essential to the accomplishment of uniform orientation with a small angular deviation (<5°). The new alignment method enabled us to execute structure analyses of axonemes by small-angle x-ray diffraction. Since this method was also useful for the quick alignment of purified microtubules, as well as tobacco mosaic tobamovirus, we expect that we can apply it to the structural analysis of many other biological filaments.

INTRODUCTION

A filamentous polymer structure is one of the most common features observed in biological materials, e.g., in the strands of DNA/RNA molecules and chains of α-helix/β-sheet structures of protein molecules. We can also observe many other specific types of biological filaments assembled from unit protein monomers, e.g., intracellular cytoskeletons, such as thin filaments and microtubules, as well as extracellular fibers, such as collagen and fibronectin. Although the structures of biological filaments and their associated components are closely related to their important functions and properties, as reviewed by Stubbs (1), the investigation of their structural details is not an easy task due to the difficulty in achieving crystallization of such long filaments. Alternatively, fiber diffraction analysis using high-energy synchrotron x-rays is one of the most powerful approaches for the observation of fine structures under physiological conditions. For x-ray fiber diffraction, however, we need to solve a crucial problem, i.e., aligning filaments in a uniform orientation to produce good diffraction peaks, thereby separating the signals corresponding to longitudinal (meridional) regularity of the filaments from those corresponding to the transverse (equatorial) structural regularity.

To align filaments for x-ray diffraction, two techniques have mainly been used thus far: slow sedimentation with low-gravity centrifugations and/or biased Brownian motions under very strong magnetic fields (1–7). Successful alignments have been shown in bacterial flagella (3), microtubules (6), tobacco mosaic tobamovirus (TMV) (1,7), and other biological fibers (2,4,5). However, these methods require a long period of time—from several hours to a few weeks—to achieve alignment, and the results are not always reproducible under various experimental conditions. Even more inconvenient, we cannot readily use these techniques for many other types of biological filaments, in particular, in cases where the filaments easily become inactive or denatured, or when some physiologically active filament components are easily degraded during alignment procedures. In this study, we modified a parallel-rotating disk instrument usually used for rheological studies and developed a quick and reproducible technique for shear-flow alignment of biological filaments. Although this technique has a resolution limit of ~1 nm^{-1} due to the orientation quality of 3–4° and to the low specimen concentrations, we successfully applied it to observe x-ray fiber diffraction of axonemes, TMV, and microtubules.

MATERIALS AND METHODS

Specimen preparation

Sperm was collected by injecting 0.55 M KCl into the body cavities of male sea urchins (*Hemicentrotus pulcherrimus* or *Anthocidaris crassispina*). The collected sperm was kept refrigerated and used for experimental purposes within 3 days. The procedures for the preparation of axonemes were based on methods used in our previous research (8). In brief, 10 mL of the collected sperm was first diluted with 0.55 M NaCl and the cell membrane was subsequently extracted by adding a 100- to 200-mL solution containing 0.08% Triton X-100, 0.4 M K-acetate, 1 mM ethylene glycol-bis-(β-aminoethyl ether)-*N*,*N*′-tetraacetic acid (EGTA), 0.1 mM ethylenediamine tetraacetic acid (EDTA), 1 mM dithiothreitol (DTT), and 10 mM Tris-HCl (pH. 8.3).

Submitted May 12, 2009, and accepted for publication September 23, 2009.

*Correspondence: skam@bio.chuo-u.ac.jp

Editor: Anne Houdusse.

0006-3495/09/12/3132/7 $2.00

doi: 10.1016/j.bpj.2009.09.041

After demembranation on ice for 1 min, spermatozoa were collected by centrifugation (4000 × *g* for 20 min; R14AF, Hitachi, Tokyo, Japan), and 30–40 slow pestle strokes in a Dounce homogenizer were given to remove sperm heads mechanically. After removing sperm heads by 60:45:30% sucrose density gradient centrifugation (9000 × *g* for 30 min; R10S, Hitachi), axonemal fragments were collected with 8000 × *g* centrifugation for x-ray diffraction analysis. For each of the experiments using sea urchin sperm axonemes, a solution containing 0.4 M K-acetate, 1 mM EGTA, 0.1 mM EDTA, 1 mM DTT, and 20 mM Tris-HCl (pH. 8.3) was used. For x-ray diffraction analysis, precipitated samples after centrifugations (9000 × *g* for 15 min) were resuspended in the same volume of buffer with or without 2% methylcellulose (M-0512, 4000 cPs; Sigma, St. Louis, MO).

Purified porcine brain tubulin (T240-B, Cytoskeleton, Denver, CO) was used to prepare microtubules. A microtubule-polymerizing medium (0.1 M PIPES, 1 mM EGTA, and 0.5 mM $MgCl_2$, pH 6.9) containing 1 mM GTP and 50 μM taxol, was added to the tubulin (final tubulin concentration, 10 mg/mL) and incubated at 37°C for 20 min. Just before x-ray diffraction experiments, the same amount of the microtubule-polymerizing medium containing 2% methylcellulose was added. Purified wild-type TMV was provided by Dr. Y. Watanabe (Department of Life Sciences, The University of Tokyo, Meguro, Tokyo). For TMV, a solution containing 1 mM EDTA and 10 mM K-phosphate buffer (pH 6.8) was used. For x-ray diffraction analysis, a pelleted sample after centrifugation (30,000 × *g* for 60 min) was resuspended in the same volume of buffer with or without 2% methylcellulose. All x-ray diffraction observations were carried out at room temperature (23–25°C).

X-ray diffraction

For the observation of x-ray diffraction patterns, we used a synchrotron radiation x-ray beam; either the beamline 15A (beam size 0.5 (V) × 1.5 (H) mm, $\lambda = 0.15$ nm) at the Photon Factory (KEK, Tsukuba, Japan) or the beamline 45XU (0.1 (V) × 0.2 (H) mm, $\lambda = 0.09$ or 0.15 nm) at the Spring-8 (JASRI, Hyougo, Japan). Diffraction intensity peaks were recorded with a Hamamatsu cooled CCD camera with 0.1- to 5.0-s exposures. A camera length ranging between 1 and 3 m was chosen depending on the range of signals we analyzed. Control observations (background) were carried out with buffer medium containing methylcellulose. We executed background subtraction and image averaging (n = 10–120) using ImageJ (ver.1.38×, Wayne Rasband, National Institutes of Health, Bethesda, MD).

Apparatus for shear-flow alignment

The apparatus used for the shear-flow alignment of axonemes and TMV was made of two stainless steel tubes (inner diameter, 16–17 mm; Nogata Denki Kogyo, Tokyo, Japan). On each tube end, a coverslip (16 or 18 mm in diameter, No. 1; Matsunami, Tokyo, Japan) or a thin Kapton film (50H, 12.5 μm thick; DuPont, Wilmington, DE) had been glued (Fig. S1 in the Supporting Material). The two tubes were then placed in a head-to-head manner, with the windows directly facing each other (Fig. 1 and Fig. S1), leaving a narrow gap (0.1–0.35 mm; Fig. S1). Coverslips or Kapton films were thus used as two parallel disks.

One of the tubes was then connected to a DC motor with a rubber belt for rotation. Before the experiments, the rate of disk rotation had been calibrated with a speed meter (testo 465, Testo AG, Lenzkirch, Germany). After placing the specimen suspension (50–100 μL) in the narrow gap between two disks, one of the tubes was rotated at a constant rate (5–20 s^{-1}; Movie S1 and Movie S2), giving a stable gradient of flow velocity (shear flow) to the suspension of specimens. When the gap between the two parallel disks was 0.15–0.25 mm, the calculated shear rate around the area 6 mm away from the axis center of rotation was 160–5000 s^{-1}.

For the microtubule experiments, we used an improved apparatus made of a direct-drive AC motor (HM2225 F12H; Technohands, Kanagawa, Japan) that had a rotating shaft with a through-hole (diameter, 22.5 mm), inside of which one of the stainless steel tubes (Fig. S1) was fixed. With this apparatus, we could execute shear-flow alignment with a wider disk gap (for larger sample amounts) and with more stable spin rates compared to the apparatus described above. In this case, a rate of rotation of up to 60 s^{-1} was possible, giving a maximum shear rate of 15,000 s^{-1}.

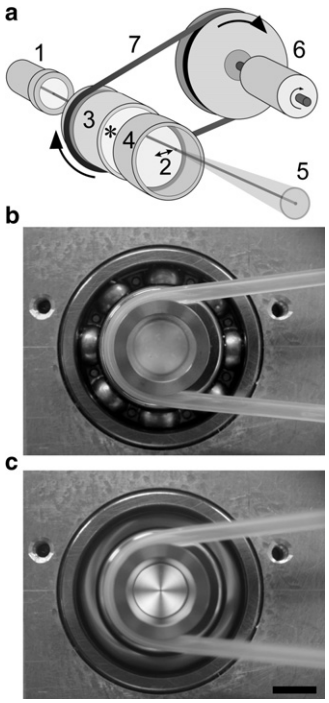

FIGURE 1 A schematic drawing and photographs showing the apparatus used for shear-flow alignment of biological filaments. (*a*) The incident x-ray beam (*1*) was passed through an area 6 mm away from the center (*2*) of a pair of disks (*3* and *4*) that were glued to stainless steel tubes (Fig. S1). Suspensions of axonemes (2–5 mg/mL), TMV (5 mg/mL), or microtubules (2–5 mg/mL), were placed between the two parallel disks (*). X-ray diffraction was measured on the downstream side (*5*). One of the disks (*3*) was rotated by a DC motor (*6*) and a rubber belt (*7*). (*b* and *c*) The apparatus was placed between two crossed polarizing plates and the specimens (axonemes) were observed through a disk window from the upstream side of the incident x-ray beam before applying shear flow (*b*) and under shear flow during rotation of the disk (*c*). A cross-shaped pattern can be clearly observed, indicating the birefringence of the specimen formed by shear flow. Occasionally, air bubbles were formed during disk rotation, but they stayed consistently near the center area of the disk. Scale bar, 10 mm.

RESULTS AND DISCUSSION

After putting the specimens between the disks, one of the disks was rotated at 5–60 s^{-1} and shear flow at a rate of 160–15,000 s^{-1} was given. During and after giving shear flow to the axoneme suspension, we observed flow birefringence of specimens, as shown in Fig. 1 *c*. This indicated that the alignment of flagellar axonemes seemed to be quickly accomplished by disk rotation to a certain extent. X-ray diffraction should give more direct evidence of this when it is used for checking the quality of alignment, as shown below.

For the x-ray diffraction experiments, we developed two types of apparatus. The first type is driven by a DC motor and a rubber belt, and was used for axonemes and TMV. The second type is directly driven by an AC motor and was used for microtubules. Higher shear rates provided better alignment, but with the inevitable problem of the sample medium being splashed away by high centrifugal forces. Thus, there was a practical limit to the available shear rates. Contamination by small bubbles or dust in the sample medium was of no concern in our experiment, because these would automatically accumulate in the center area of the chamber. For the rotating disk materials, coverslips offered better results, as judged from the quality of fiber alignment, probably due to mechanical stability; however, when an x ray of 0.15 nm wavelength was used, we had to choose Kapton films, which had a lower rate of absorption than the coverslips.

Axonemes contain >200 polypeptides (9,10), and some major components are regularly arranged along the longitudinal axis (11). Therefore, axonemes were chosen to test our alignment technique, as they are well suited to this type of diffraction study. To date, fine structures of the specific 9 + 2 bundle of microtubules and dynein arms have been described only by electron microscopy studies (12–16). In particular, recent cryoelectron tomography studies (13–16) reveal the detailed molecular arrangements of axonemes. To understand the motility mechanisms of cilia and flagella (17), it is crucial to investigate dynamic structural changes that take place under physiological conditions, e.g., how the axonemal structure changes by the motility activators, blockers, or regulators (ATP, vanadate, Ca^{2+}, and so on). Such dynamic features are more suitably targeted by x-ray diffraction analysis than by electron microscopy techniques. Furthermore, with the recent attention to the biomedical significance of ciliary and flagellar functions (18,19), axonemes would be one of the most interesting specimens for x-ray diffraction analysis.

The main components of axonemes that would diffract x-rays are tubulin (~4 or ~8 nm longitudinal periodicity), radial spokes (~96 nm), and dynein arms (~24 or ~96 nm), which compose >90% of all axonemal proteins (9). Diffraction intensities from these components are useful quantitative indicators of how well axonemal filaments are aligned to a given shear flow.

Movie S3 and Movie S4 show how the observed diffraction pattern changed when we gave shear flow to the specimen. As shown by the first several frames of each movie (*yellow marks*), x-ray diffraction was observed as a Debye-Scherrer ring pattern before we applied shear flow to the axonemal suspension. The average diffraction pattern shown in Fig. 2 *a* shows a similar result. Like x-ray solution scattering, there were no prominent intensity peaks in either the equatorial or the meridional direction, implying that axonemal orientation was completely random in the suspension. When we initiated disk rotation, the diffraction pattern changed (Movie S3 and Fig. 2 *b*), which indicates partial alignment of axonemes by application of shear flow to the specimen suspension. However, due to the angular deviation of >20°, we could not use the obtained data for further detailed diffraction analysis. This indicates that giving shear flow to the medium was not sufficient for alignment of axonemes.

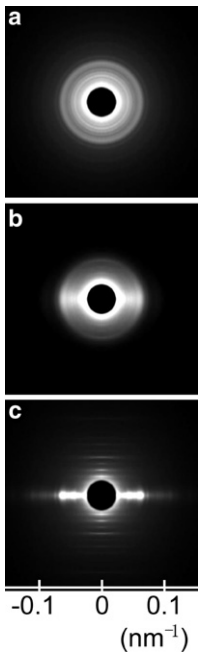

FIGURE 2 Examples of observed x-ray diffraction patterns ($\lambda = 0.15$ nm; exposure time, 30 s). The vertical axis in each diffraction pattern corresponds to the circumferential direction of the parallel disks. (*a–c*) Diffraction patterns (reciprocal spacing up to 0.142 nm^{-1}) observed with the suspension of axonemes isolated from sea urchin (*A. crassispina*) sperm flagella before applying shear flow (*a*), during application of shear flow in a medium without methylcellulose (*b*), and during application of shear flow in a medium containing 1% methylcellulose (*c*). Obvious differences between diffraction patterns in the meridional and equatorial directions are shown.

A prominent and quick aligning effect was unexpectedly discovered by adding methylcellulose (~1%) to the medium. Clear diffraction peaks corresponding to the reciprocal spacing of ~0.125, ~0.063, and ~0.042 nm^{-1} (corresponding to the ~8-, ~16-, and ~24-nm axial periodicity in the axonemes, respectively) were observed as sharp layer lines in the direction of flow (Movie S4, and Figs. 2 *c* and 3). We also observed the meridional reflection at ~0.25 nm^{-1}, indicating helical arrangements of tubulin molecules in axonemal microtubules. We concluded that axonemes were aligned almost uniformly in the direction of flow, since all of these meridional layer lines were as expected from the longitudinal regularity of axonemal components, as shown by the theoretical calculation (20).

As no osmotic effects of methylcellulose (21) forming filament bundles were observed in our preparations (Fig. S2), the observed equatorial diffractions were not caused by

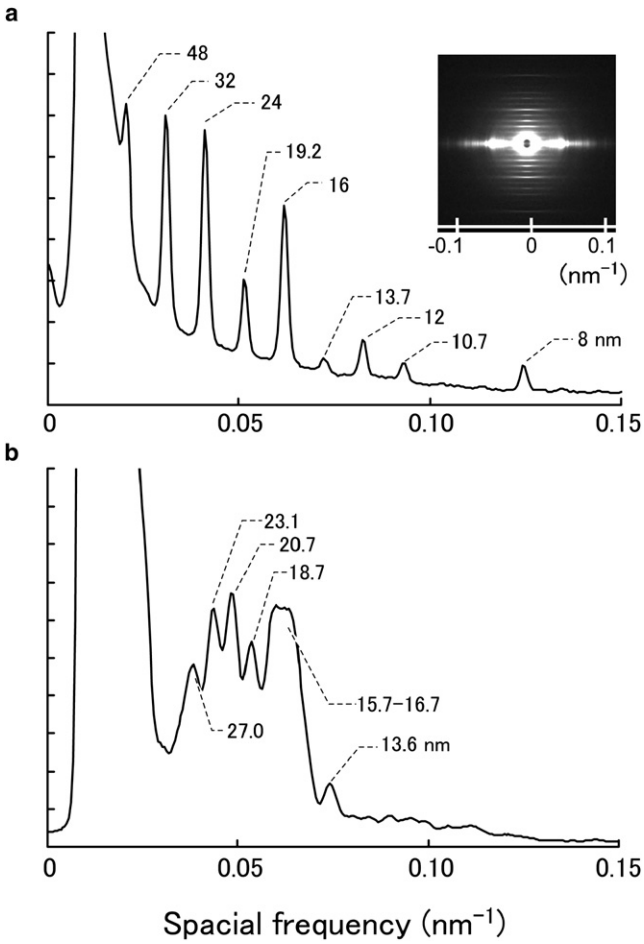

FIGURE 3 Detailed analysis of the diffraction pattern (<0.18 nm^{-1}; $\lambda = 0.09$ nm) of axonemes isolated from sea urchin (*H. pulcherrimus*) sperm flagella. Profiles of diffraction intensity on the meridian (*a*) and on the equator (*b*) are shown. The meridional peaks are indexed as orders of 96 nm. The same scale was used for the equator.

interference effects between adjacent axonemes. To confirm this observation, we calculated rotational averages of obtained diffractions and compared the intensity profile of the specimen with to that of the specimen without methylcellulose (Fig. S3). No specific peak was induced by adding methylcellulose in the observed range (<0.15 nm^{-1}). With the medium alone, we could not find any specific diffraction peaks in the x-ray scattering with or without methylcellulose. Thus, it is suggested that the observed equatorial peaks (Fig. 3 *b*) originate from the distribution of the entire axonemal mass, which is projected onto the plane perpendicular to the axonemal axis. From the angular spreading of equatorial peak intensities, we estimated the angular deviation of the filament alignment to be <5°.

Although we could not determine the exact reasons, adding methylcellulose to the medium of axonemal suspension was highly effective in facilitating flow-induced alignment. Under the conditions used here, alignment was accomplished within 5 s (Movie S4). Without methylcellulose, alignment was not improved even by prolonged (>5 min) application of shear flow. As the diffraction pattern becomes gradually obscured after the cessation of disk rotation, continuous application of shear flow is crucial. A higher shear rate (>1000 s^{-1}) and methylcellulose with a higher molecular mass (4000 cPs > 400 cPs) provided better results. Polyvinylpyrrolidone (10%) had a similar effect.

Under shear-flow conditions, rigid slender bodies suspended in a medium should align with the flow, according to theoretical investigations by Jeffery (22) and experimental demonstrations by Stover et al. (23). However, our experiments without methylcellulose showed poor alignment in the case of axonemes (Fig. 2 *b* and Movie S3), even when a very high shear rate was employed (>1000 s^{-1}). Therefore, applying shear flow alone is not sufficient to align axonemes. Although polymer effects on the Jeffery orbit have been experimentally investigated (24), the conditions used in that study seemed to be quite different from ours. Furthermore, the rheological parameters used in our experiments have not been well examined so far, either theoretically or experimentally (25,26), e.g., a high shear rate (>1000 s^{-1}) and a filament number concentration of 0.02 μm^{-3} (2–5 mg/mL, 5–20 axonemes of mean length 10 μm in 1000 μm^3) under semidiluted conditions (~20 nL^3). Thus, the effects of methylcellulose found in this study had not previously been clear.

Aqueous polymers would have complicated effects on the medium, e.g., enhanced viscosity, reduced flow turbulence, molecular crowding, and non-Newtonian flow-thinning. The concentrations of protein (0.2–0.5%) and methylcellulose (1%) used in this study were 10 times lower than those defined by Zimmermann (27) and Ellis (28) as crowding conditions (20–30%). We found no evidence in the case of axonemes to show bundling by methylcellulose (Fig. S2 and Fig. S3). Thus, we speculated that viscosity would be more crucial for shear-flow alignment under our experimental conditions than the effects of macromolecular crowding. We estimated the Reynolds number (Re) under our experimental conditions to be 0.054–0.36 using the equation

$$\mathrm{Re} = \frac{\rho \times L \times v}{\eta} = \frac{1 \times 10^3 (\mathrm{kg/m^3}) \times 3 \sim 4 \times 10^{-4} (\mathrm{m}) \times 0.36 \sim 1.8\ (\mathrm{m/s})}{2\ (\mathrm{kg/m \cdot s})},$$

where ρ, L, v, and η are the fluid density, the gap between the two disks, the maximum flow rate, and the dynamic

viscosity, respectively. This suggests that adding methylcellulose seems to be effective in reducing the Re to <1 and would stabilize the creeping flows in our alignment chamber. However, decreasing the Re would not be sufficient to accomplish fiber alignment, because, as we also observed, the higher rates of disk rotation provided better results. Further precise investigations should be conducted to find better aligning conditions. Although the rheological background is still unclear, similar medium conditions involving aqueous polymers would be useful in facilitating fiber alignment in other shear-flow techniques (29–33).

In the case of axonemes, high shear rates of 1000–6000 s^{-1} that were prolonged for up to 15 min gave no apparent change in x-ray diffraction, indicating that there was no apparent mechanical damage to the structure by shear forces. Shear forces applied to axonemes, estimated to be less than the order of 10 nN, and would have little effect on the dynein motors on doublet microtubules.

We next tested how the technique described here could be useful for other types of biological fibers. We chose TMV as a stable material, the structure of which has already been well described (7), and purified taxol-stabilized microtubules and F-actin as unstable labile fibers. In the cases of TMV and microtubules, our method was effective, and alignment was completed within 5 s after initiating disk rotation. Preliminary trials with F-actin have not yet been successful.

In the case of TMV, low-angle equatorial signals of ~0.04 nm^{-1}, corresponding to the tube diameter of TMV, were clearly observed (Fig. 4), as were almost all of the diffraction intensity peaks described in previous works (7). Here, the observation by Bernal and Fankuchen (34) was reproduced, although they did not use methylcellulose. In the diffraction pattern recorded with a higher resolution (Fig. 4 *c*), we could see split layer lines. Although some of these lines would come from the helical arrangement of components of TMV, a more likely explanation is that TMV has specific features that cause it to behave like liquid crystals. Our observation suggests that significant fractions of TMV were in such a nematic crystal phase even under dynamic shear-flow conditions. In previous studies using the capillary tube method (34), similar features were described.

The results with microtubules are shown in Fig. 5 and in Fig. S4. In the case of microtubules, we again needed to include methylcellulose to accomplish alignment. By using the standard diffraction intensity peak of Ag-behenate (5.838 nm), we determined the tubulin axial periodicity to be 4.05 ± 0.05 nm ($n = 5$). This value is almost equal to previous estimates (4.05–4.09 nm) determined by x-ray diffraction analyses using conventional aligning methods (6,35) or native axonal microtubules (36). We compared the position of the meridional reflections of tubulin with those in sea-urchin sperm axonemes, observations which were carried out under exactly the same experimental conditions (Fig. S4), and we concluded that there was no difference between the two materials in axial periodicity of tubulin. From these observations, we determined, more precisely, that the reciprocal spacings in the axonemes were 0.123 and 0.0412 nm^{-1} (corresponding to 8.1 and 24.3 nm periodicity, respectively), rather than ~0.125 and ~0.042 nm^{-1}, the rough calculations from the inverse of periodicity of tubulin dimers and dynein arms

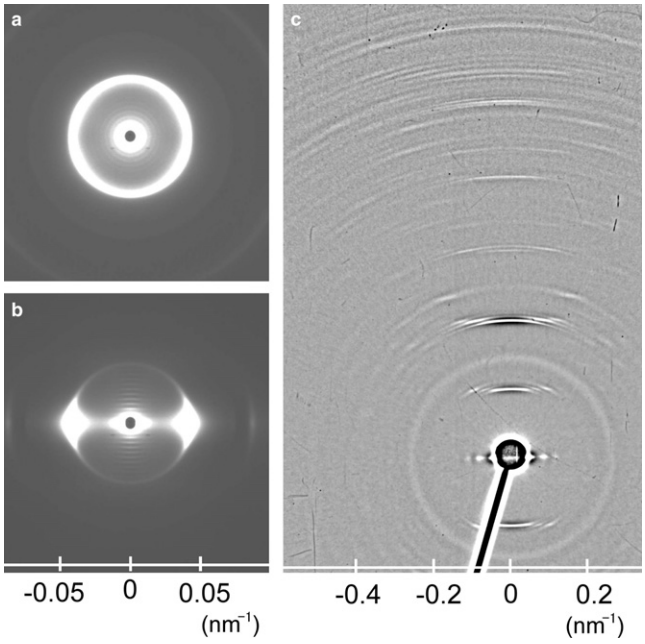

FIGURE 4 Diffraction patterns (<0.09 nm^{-1}, $\lambda = 0.09$ nm) of TMV suspended in a medium that contained 1% methylcellulose. (*a*) The pattern before applying shear flow. (*b*) The pattern during application of shear flow to the specimen. (*c*) The pattern during application of shear flow, but with a higher range of diffraction angle (<1.1 nm^{-1}). The latter pattern was recorded after an exposure time of 10 min on an image plate (BAS-IP MS2025, Fuji Film) placed 390 mm from the specimen.

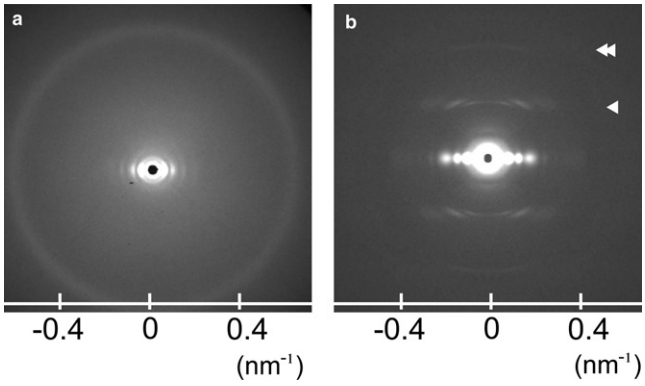

FIGURE 5 Diffraction pattern (<0.67 nm^{-1}, $\lambda = 0.09$ nm) from taxol-stabilized microtubules in a medium containing 1% methylcellulose, averaged from 50 images recorded with 2-s exposures. (*a*) The pattern before applying shear flow (averaged from five images at 2 s exposure). (*b*) The pattern during application of shear flow to the specimen (averaged from 50 images). The spacings of two layer lines, indicated by the single and double arrowheads, were obtained as 4.05 and 2.03 nm, respectively, after the x-ray optics was calibrated for diffraction from Ag-behenate.

(corresponding to ~8 and ~24 nm, respectively). The difference in angular deviation between the two aligned specimens implies that some other factors, e.g., fiber length, diameter, or mechanical rigidity, are crucial to the efficiency of shear-flow alignment.

The lateral spacing of Bessel terms J_1–J_3 and J_{13} (6), which originate from the microtubule structure, were measured as 0.050 ± 0.001, 0.84 ± 0.002, 0.126 ± 0.003, and 0.169 ± 0.003 nm^{-1}, respectively. By comparing these data with those from the simulation of diffraction patterns of 13 protofilaments with the three-start helical arrangement of globular tubulin (data not shown), we estimated the diameter of the circle connecting the centers of protofilaments to be 24.4 ± 0.6 nm ($n = 4$), which is consistent with estimates by diffraction analysis using conventional aligning methods (6,35).

This study provides us with what we believe to be a novel and powerful technique in the field of x-ray fiber diffraction that has three important advantages over other techniques. First, we need only to put the specimen suspension between two parallel disks and start the rotation. As specimens become aligned in seconds, quick surveys of diffraction patterns and structural analysis can then be executed in a few minutes. Thus, our method may be useful even for physiologically unstable filaments, and accumulation of irradiation damage from x-rays would be negligible, as the medium is being stirred continuously. For example, we were able to obtain preliminary data to compare the structural differences between stable GMPCPP (a slowly hydrolyzable GTP analog) and unstable GTP microtubules. The meridional 8-nm reflection intensity appeared only in conventional GTP microtubules (data not shown), which are assumed to consist mostly of GDP tubulin. This may indicate structural differences between GDP and GTP tubulin in microtubules. Such experiments were impossible using conventional fiber alignment techniques. Second, the quality of alignment was better than or at least equivalent to that of conventional techniques (2–7,35). With the limit of resolution (~1 nm^{-1}) and quality of orientation (3–4°) in this study, we cannot directly determine the details of molecular structures, but we expect to be able to answer many cell biology questions on the dynamic features of filamentous structure. Third, using our technique, a small volume (50–100 μL) of specimen is enough for the diffraction measurement. By modifying the chamber design, 10–20 μL would practically be possible. Compared with other methods of shear-flow alignment, e.g., Couette flow cells (30,31) or extensional flow cells (32,33), the method introduced here would be more useful for small-volume specimens. We expect that we could apply the technique to many other biological filaments, even in cases where only a small amount of specimen is available. Further application would be possible with many other biological filaments, including filamentous viruses, paired helical filaments, and amyloid fibrils of medical significance (31,36–39).

SUPPORTING MATERIAL

Four figures and four movies are available at http://www.biophysj.org/biophysj/supplemental/S0006-3495(09)01525-2.

The authors are grateful to Dr. Naoki Sasaki (Hokkaido University) for his critical reading of our MS. The experiments were performed with the approval of the Photon Factory Program Advisory Committee (2004G390, 2005G310) and the SPring-8 Proposal Review Committee (2005B0075, 2006A1175, 2006B1498, 2007A1590, 2007B1470, 2008A1444, and 2009A1032). The authors thank the Misaki Marine Biological Station at The University of Tokyo, and the Marine and Coastal Research Center at Ochanomizu University, as well as Mr. Fumio Matsuzawa (Fumi-Maru, Manazuru, Kanagawa, Japan), for supplying the sea urchins used in this study. We also thank Dr. Y. Watanabe (Department of Life Sciences, The University of Tokyo, Komaba, Tokyo) for kindly providing TMV.

This work was supported by Grants in Aid for Exploratory Research (20657014) and for Scientific Research on Priority Areas (1704911, 19037010) from The Ministry of Education, Culture, Sports, Science and Technology of Japan (MEXT) and by the program of Creation and Application of ''Soft Nano-Machine'', the Hyperfunctional Molecular Machine (Core Research for Evolutional Science and Technology, Japan Science and Technology Agency).

REFERENCES

1. Stubbs, G. 1999. Developments in fiber diffraction. *Curr. Opin. Struct. Biol.* 9:615–619.
2. Torbet, J. 1987. Using magnetic orientation to study structure and assembly. *Trends Biochem. Sci.* 12:327–330.
3. Yamashita, I., H. Suzuki, and K. Namba. 1998. Multiple-step method for making exceptionally well-oriented liquid-crystalline sols of macromolecular assemblies. *J. Mol. Biol.* 278:609–615.
4. Oda, T., K. Makino, I. Yamashita, K. Namba, and Y. Maéda. 1998. Effect of the length and effective diameter of F-actin on the filament orientation in liquid crystalline sols measured by x-ray fiber diffraction. *Biophys. J.* 75:2672–2681.
5. Popp, D., V. V. Lednev, and W. Jahn. 1987. Methods of preparing well oriented sols of f-actin containing filaments suitable for fiber diffraction. *J. Mol. Biol.* 197:679–684.
6. Bras, W., G. P. Diakun, J. F. Diaz, G. Maret, H. Krarmer, et al. 1998. The susceptibility of pure tubulin to high magnetic fields: a magnetic birefringence and x-ray fiber diffraction study. *Biophys. J.* 74:1509–1521.
7. Namba, K., R. Pattanayek, and G. Stubbs. 1989. Visualization of protein-nucleic acid interactions in a virus. Refined structure of intact tobacco mosaic virus at 2.9 Å resolution by x-ray fiber diffraction. *J. Mol. Biol.* 208:307–325.
8. Kamimura, S., M. Yano, and H. Shimizu. 1985. ATP hydrolysis coupled to microtubule sliding in sea-urchin sperm flagella. *J. Biochem.* 7:1509–1515.
9. Luck, D. J. L. 1984. Genetic and biochemical dissection of the eukaryotic flagellum. *J. Cell Biol.* 98:789–794.
10. Gregory, J., G. J. Pazour, N. Agrin, J. Leszyk, and G. B. Witman. 2005. Proteomic analysis of a eukaryotic cilium. *J. Cell Biol.* 170: 103–113.
11. Warner, F. D., and P. Satir. 1974. The structural basis of ciliary bend formation. Radial spoke positional changes accompanying microtubule sliding. *J. Cell Biol.* 63:35–63.
12. Goodenough, U. W., and J. E. Heuser. 1982. The substructure of the outer dynein arm. *J. Cell Biol.* 95:798–815.
13. Nicastro, D., J. R. McIntosh, and W. Baumeister. 2005. 3D structure of eukaryotic flagella in a quiescent state revealed by cryo-electron tomography. *Proc. Natl. Acad. Sci. USA.* 102:15889–15894.

14. Nicastro, D., C. Schwartz, J. Pierson, R. Gaudette, M. E. Porter, et al. 2006. The molecular architecture of axonemes revealed by cryoelectron tomography. *Science*. 313:944–948.

15. Ishikawa, T., H. Sakakibara, and K. Oiwa. 2007. The architecture of outer dynein arms in situ. *J. Mol. Biol.* 368:1249–1258.

16. Bui, K. H., H. Sakakibara, T. Movassagh, K. Oiwa, and T. Ishikawa. 2009. Asymmetry of inner dynein arms and inter-doublet links in *Chlamydomonas* flagella. *J. Cell Biol.* 186:437–446.

17. Lindemann, C. B., and K. S. Kanous. 1997. A model for flagellar motility. *Int. Rev. Cytol.* 173:1–72.

18. Badano, J. L., N. Mitsuma, P. L. Bales, and N. Katsanis. 2006. The ciliopathies: an emerging class of human genetic disorder. *Annu. Rev. Genomics Hum. Genet.* 7:125–148.

19. Fliegauf, M. M., T. Benzing, and H. Omran. 2007. When cilia go bad: cilia defects and ciliopathies. *Nat. Rev. Mol. Cell Biol.* 8:880–893.

20. Iwamoto, H. 2008. Theory of diffraction from eukaryotic flagellar axonemes. *Cell Motil. Cytoskeleton.* 65:563–571.

21. Asakura, S., and F. Oosawa. 1954. On interaction between two bodies immersed in a solution of macromolecules. *J. Chem. Phys.* 22:1255–1256.

22. Jeffery, G. B. 1922. The motion of ellipsoidal particles immersed in a viscous fluid. *Proc. R. Soc. Lond. A.* 102:161–179.

23. Stover, C. A., D. L. Koch, and C. Cohen. 1992. Observations of fiber orientation in simple shear flow of semi-dilute suspensions. *J. Fluid Mech.* 238:277–296.

24. Iso, Y., D. L. Koch, and C. Cohen. 1996. Orientation in simple shear flow of semi-dilute fiber suspensions. 1. Weakly elastic fluids. *J. Non-Newt. Fluid Mech.* 62:115–134.

25. Azaiez, J., R. Guénette, and A. Ait-Kadi. 1997. Investigation of the abrupt contraction flow of fiber suspensions in polymeric fluids. *J. Non-Newt. Fluid Mech.* 73:289–316.

26. Larson, R. G. 1999. The Structure and Rheology of Complex Fluids. Oxford University Press, Oxford, United Kingdom.

27. Zimmerman, S. B., and S. O. Trach. 1991. Estimation of macromolecule concentrations and excluded volume effects for the cytoplasm of *Escherichia coli*. *J. Mol. Biol.* 5:599–620.

28. Ellis, R. J. 2001. Macromolecular crowding: obvious but underappreciated. *Trends Biochem. Sci.* 26:597–604.

29. Fairhurst, C. F., M. C. Holmes, and M. S. Leaver. 1996. Shear alignment of a rhombohedral mesh phase inaqueous mixtures of a long chain nonionic surfactant. *Langmuir*. 12:6336–6340.

30. Marrington, R., T. R. Dafforn, D. J. Halsall, J. I. MacDonald, M. Hicks, et al. 2005. Validation of new microvolume Couette flow linear dichroism cells. *Analyst (Lond.).* 130:1608–1616.

31. Hill, E. K., B. Krebs, D. G. Goodall, G. J. Howlett, and D. E. Dunstan. 2006. Shear flow induces amyloid fibril formation. *Biomacromolecules*. 7:10–13.

32. Kisilak, M., H. Anderson, N. S. Babcock, and M. R. Stetzer. 2001. An x-ray extensional flow cell. *Rev. Sci. Instrum.* 72:4305–4307.

33. Rennie, A. R., S. Baré, J. K. Cockcroft, and A. C. Jupe. 2006. Characterization of the flow of anisotropic colloidal particles using energy-dispersive x-ray diffraction. *J. Colloid Interface Sci.* 293:475–482.

34. Bernal, J. D., and I. Fankuchen. 1941. X-ray and crystallographic studies of plant virus preparations. *J. Gen. Physiol.* 25:111–146.

35. Mandelkow, E., J. Thomas, and C. Cohen. 1977. Microtubule structure at low resolution by x-ray diffraction. *Proc. Natl. Acad. Sci. USA*. 74:3370–3374.

36. Wais-Steider, C., N. S. White, D. S. Gilbert, and P. M. Eagles. 1987. X-ray diffraction patterns from microtubules and neurofilaments in axoplasm. *J. Mol. Biol.* 197:205–218.

37. Serpell, L., J. Berriman, R. Jakes, M. Goedert, and R. A. Crowther. 2000. Fiber diffraction of synthetic α-synuclein filaments shows amyloid-like cross-β conformation. *Proc. Natl. Acad. Sci. USA*. 97:4897–4902.

38. Warren, J., W. J. Goux, L. Kopplin, A. D. Nguyen, K. Leak, et al. 2004. The formation of straight and twisted filaments from short tau peptides. *J. Biol. Chem.* 279:26868–26875.

39. von Bergen, M., S. Barghorn, J. Biernat, E. M. Mandelkow, and E. Mandelkow. 2005. Tau aggregation is driven by a transition from random coil to β-sheet structure. *Biochim. Biophys. Acta.* 1739:158–166.